

## Colossal negative thermal expansion induced by magnetic phase competition on frustrated lattices in Laves phase compound (Hf,Ta)Fe<sub>2</sub>

B. Li,<sup>1,\*</sup> X. H. Luo,<sup>2</sup> H. Wang,<sup>3</sup> W. J. Ren,<sup>2,†</sup> S. Yano,<sup>4</sup> C.-W. Wang,<sup>4</sup> J. S. Gardner,<sup>4</sup> K.-D. Liss,<sup>5</sup> P. Miao,<sup>6</sup> S.-H. Lee,<sup>6</sup> T. Kamiyama,<sup>6</sup> R. Q. Wu,<sup>3</sup> Y. Kawakita,<sup>1</sup> and Z. D. Zhang<sup>2</sup>

<sup>1</sup>Japan Proton Accelerator Research Complex, Japan Atomic Energy Agency, Tokai, Ibaraki 319-1195, Japan

<sup>2</sup>Shenyang National Laboratory for Material Sciences, Institute of Metal Research, Chinese Academy of Sciences, Shenyang 110016, China

<sup>3</sup>Department of Physics and Astronomy, University of California, Irvine, California 92697, USA

<sup>4</sup>Neutron Group, National Synchrotron Radiation Research Center, Hsinchu 30077, Taiwan

<sup>5</sup>Australian Nuclear Science and Technology Organisation, Lucas Heights, New South Wales 2234, Australia

<sup>6</sup>Neutron Science Laboratory, Institute of Materials Structure Science, High Energy Accelerator Research Organization, Tsukuba, Ibaraki 305-0801, Japan

(Received 10 March 2016; published 6 June 2016)

Competition between ferromagnetic and antiferromagnetic phases on frustrated lattices in hexagonal Laves phase compound Hf<sub>0.86</sub>Ta<sub>0.14</sub>Fe<sub>2</sub> is investigated by using neutron diffraction as a function of temperature and magnetic fields and density-functional-theory calculations. At 325 K, the compound orders into the 120° frustrated antiferromagnetic state with a well-reduced magnetic moment, and an in-plane lattice contraction simultaneously sets in. With further cooling down, however, the accumulated distortion in turn destabilizes this susceptible frustrated structure. The frustration is completely relieved at 255 K when the first-order transition to the ferromagnetic state takes place, where a colossal negative volumetric thermal expansion,  $-123 \times 10^{-6}/\text{K}$ , is obtained. Meanwhile, the antiferromagnetic state can be suppressed by few-tesla magnetic fields, which results in a colossal positive magnetostriction. Such delicate competition is attributed to the giant magnetic fluctuation inherent in the frustrated antiferromagnetic state. Therefore, the magnetoelastic instability is approached even under a small perturbation.

DOI: [10.1103/PhysRevB.93.224405](https://doi.org/10.1103/PhysRevB.93.224405)

### I. INTRODUCTION

The magnetic phase competition due to comparable interactions dominates a wide variety of important magnetic phenomena [1,2]. The subtle compromise among individual phases gives rise to rich magnetic phase diagrams. In the vicinity of phase boundaries, moderate magnetic fields can induce a giant response, which is the origin of plenty of magnetic properties such as colossal magnetoresistance [1–4]. Magnetic frustration leading to high degeneracies usually promotes such competition, and more intriguing magnetic behaviors are expected [5–7]. Taking the competition between ferromagnetic (FM) and antiferromagnetic (AFM) interactions as an example, the theoretical study suggests that a transition occurs from FM metal to paramagnetic (PM) metal on the geometrically frustrated pyrochlore lattice, rather than to the AFM insulator in the absence of the frustration effect [8]. Given that magnetic frustration is typically relieved to some extent via the lattice distortion [6,9], the interesting question of how the lattice degree of freedom is influenced by this competition is raised. Peculiarly, negative thermal expansion (NTE) effects are sometimes accompanied by ordering of frustrated magnetic moments [10], such as in YMn<sub>2</sub> [11,12], Mn<sub>3</sub>(Gu,Ge)N [13], and ZnCr<sub>2</sub>Se<sub>4</sub> [14].

To this end, the magnetoelastic pseudobinary Laves phase compounds Hf<sub>1-x</sub>Ta<sub>x</sub>Fe<sub>2</sub>, crystallizing in the geometrically frustrated hexagonal MgZn<sub>2</sub>-type structure, are probably an ideal playground [15–18]. As shown in Fig. 1(a), this is a

robust frustrated system in which kagome-lattice layers formed by Fe ions occupying  $6h$  sites and triangle-lattice layers of Fe ions located at  $2a$  sites alternately repeat along the  $c$  direction. The intrinsic magnetism remains inconclusive, in spite of many attempts to study magnetization [15], <sup>57</sup>Fe Mössbauer spectra [15,16], and neutron diffraction [17,18]. Note that no magnetic superlattice diffraction was observed in the neutron diffraction measurements. When  $0.12 \leq x \leq 0.25$ , two transitions successively take place as temperature decreases, and the latter is accompanied by a NTE suggested by an earlier laboratory x-ray diffraction study [15]. Its large volumetric change is comparable to that of leading present-day NTE materials [19].

To determine the magnetic structures and understand their coupling with the lattice, we conducted a comprehensive study by combining high-resolution x-ray diffraction and neutron diffraction and high-intensity neutron diffraction with complementary density-functional-theory (DFT) calculations. It is revealed that the colossal NTE with a coefficient of volumetric thermal expansion as large as  $-123 \times 10^{-6}/\text{K}$  is induced by the first-order magnetic transition from frustrated AFM to collinear FM states with the crystal symmetry preserved. Our study unambiguously indicates that magnetic frustration plays a crucial role in the NTE of this system and sheds light on searching for NTE materials by tuning the competing magnetic orders on frustrated lattices.

### II. EXPERIMENTS AND CALCULATIONS

The polycrystalline ingot was prepared by arc melting the constituent elements with 99.9% purity. The temperature-dependent high-resolution x-ray diffraction was carried out

\*bing.li@j-parc.jp

†wjren@imr.ac.cn

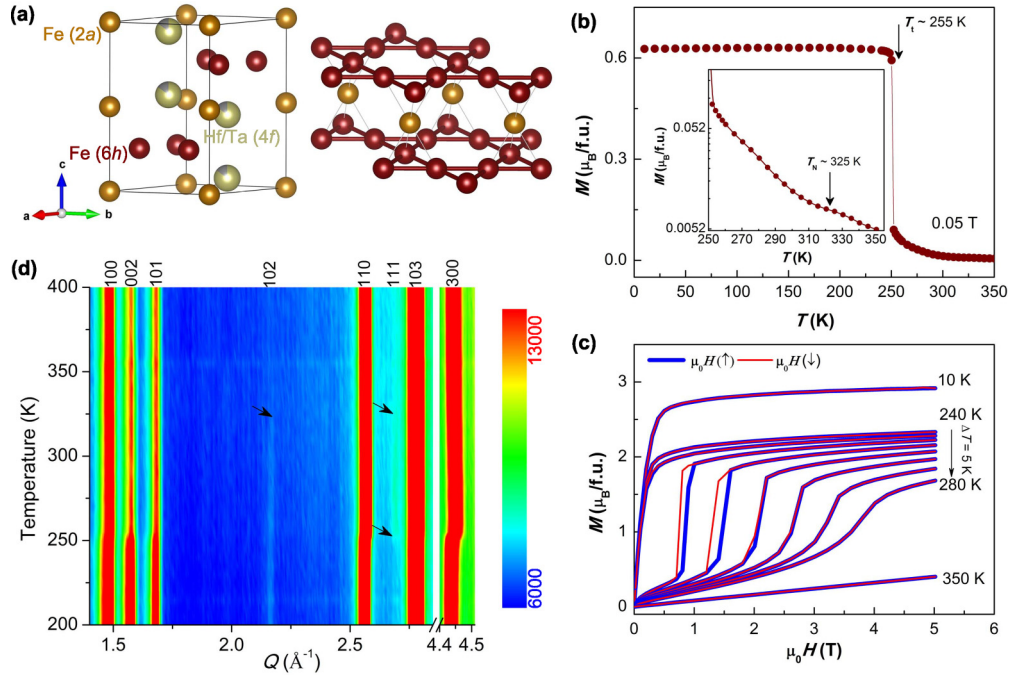


FIG. 1. (a) The crystal structure of  $\text{Hf}_{1-x}\text{Ta}_x\text{Fe}_2$ . (b) The temperature dependence of magnetization per chemical formula. The inset shows the variation around 325 K. (c) The magnetic isotherms at selected temperatures with magnetic fields increasing and decreasing labeled by arrows. (d) The contour plot of neutron diffraction intensity. The feature temperatures are pointed out by the arrows.

with Cu  $K_\alpha$  radiation on a Rigaku SmartLab diffractometer equipped with a low-temperature stage. Within the instrumental resolution of  $\Delta d/d$  of 0.2%–0.5%, no symmetry breaking is identified [20]. The magnetization was measured by using a Quantum Design MPMS XL. Two transitions were found at 325 and 255 K and are labeled as  $T_N$  and  $T_I$  in Fig. 1(b), respectively. As shown in Fig. 1(c), the field dependence of magnetization appears as the typical FM behavior at 10 K but as a magnetic-field-induced transition with hysteresis between  $T_I$  and  $T_N$ . Neutron diffraction patterns with  $\lambda = 2.4 \text{ \AA}$  were collected at the high-intensity diffractometer Wombat with a 6-T magnet and at the high-resolution diffractometer Echidna of the Australian Nuclear Science and Technology Organisation (ANSTO) [21,22]. Such a combination allows us to thoroughly determine the structures. The diffraction data were analyzed by using the Rietveld refinement method in FULLPROF [23]. SARAH [24] was utilized for the magnetic representational analysis. The composition was evaluated to be  $\text{Hf}_{0.86}\text{Ta}_{0.14}\text{Fe}_2$  by the Rietveld refinement.

DFT simulations were performed with the Vienna Ab initio Simulation Package (VASP) [25–28]. The spin-polarized generalized gradient approximation (GGA) was used for the description of the exchange-correlation interaction among electrons [29]. We treated Hf  $5d6s$ , Ta  $5d6s$ , and Fe  $3d4s$  as valence states and adopted the projector augmented-wave (PAW) pseudopotentials to represent the effect of their ionic cores [30,31]. To simulate the noncollinear AFM structure, the noncollinear magnetic mode was adopted with a negligible penalty contribution to the total energy added to the Hamiltonian in order to keep the noncollinear local moment in the kagome-lattice plane [32]. The energy cutoff for the plane-wave expansion was 500 eV, sufficient for a transition-metal-compound system according to our test calculations.

Structures were optimized with the criteria that the atomic force on each atom became weaker than  $0.01 \text{ eV/\AA}$  and the energy convergence was better than  $10^{-6} \text{ eV}$ .

### III. RESULTS AND DISCUSSION

#### A. Neutron powder diffraction

In Fig. 1(d), we display the contour plot of diffraction intensity as a function of diffraction vector  $Q$  in the temperature window from 200 to 400 K. The Bragg peaks are labeled with their Miller indices. With increasing temperature, the intensity of the 002 peak drops dramatically at about 255 K, whereas the 300 peak exhibits a striking shift to higher  $Q$ . At the same time, a very weak peak suddenly sets in to the left of the 103 peak, which is identified as 111 peak. As temperature increases further, both the 102 and 111 peaks vanish around 325 K. The significant enhancement of intensity of the 002 peak implies that magnetic moments lie in the  $ab$  plane in the low-temperature phase. The presence of the 111 peak in the intermediate phase indicates that this compound is most likely AFM because it is not crystallographically allowed in the  $P6_3/mmc$  space group and there is no crystal structural transition identified in both x-ray and neutron diffraction measurements down to 4 K. These variations are also shown in Fig. 2(a) at selected temperatures. The feature temperatures above are very consistent with ones found in the temperature dependence of magnetization [Fig. 1(b)].

To completely determine the magnetic structures, we investigate the diffraction data at very low  $Q$ . The absence of a superlattice diffraction peak suggests the propagation vector is  $(0,0,0)$ . Thus, we carry out complete magnetic representational analysis of the space group  $P6_3/mmc$  with this propagation vector. There are two FM arrangements allowed: one with

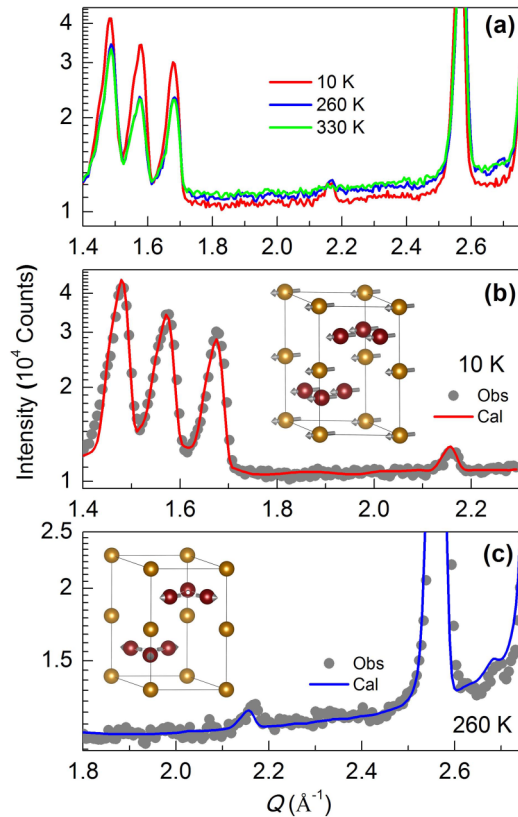


FIG. 2. (a) The neutron powder diffraction patterns at 10, 260, and 330 K. (b) and (c) The refinements of the data at 10 K ( $R_p = 4.01\%$ ,  $R_{wp} = 6.32\%$ ) and at 260 K ( $R_p = 5.98\%$ ,  $R_{wp} = 9.60\%$ ) with magnetic models that are shown as insets.

moments pointing in the  $ab$  plane and another with moments along the  $c$  axis. The latter is excluded because the simulation with this model yields stronger magnetic intensity at the positions of the 100 and 101 peaks, which is distinct from the experimentally intense 002 magnetic peak [20]. However, the in-plane model is able to reproduce these features [20]. The refinement achieved by including this in-plane magnetic model, without constraints on the moments at two sites, is shown in Fig. 2(b). The unfitted intensity around  $1.4 \text{ \AA}^{-1}$  might come from the tiny amount of impurity in our sample. The determined magnetic moments of Fe at the  $2a$  and  $6h$  sites are pretty close, and they are about  $1.42(7)\mu_B$  at 10 K and  $1.16(7)\mu_B$  at 240 K. They are converted to  $2.84\mu_B$  and  $2.32\mu_B$  for one chemical formula, very consistent with the values of  $2.9\mu_B$  and  $2.3\mu_B$  found at 10 and 240 K under magnetic fields of 5 T in magnetization measurements, respectively. Note that 240 K is just a few K lower than  $T_t$ .

We turn our attention to the AFM state where the magnetic moments of Fe at  $2a$  sites are disordered, as suggested by Mössbauer spectra measurements [16]. The diffraction patterns are compared at 260 and 330 K. The first three Bragg peaks show nearly constant intensities. The identified differences are associated with the 102 and 111 peaks, even though they are quite weak. In fact, the 111 peak is not present in either our high-resolution diffraction pattern taken at Echidna (not shown here) or previous neutron powder diffraction measurements with almost two orders of magnitude

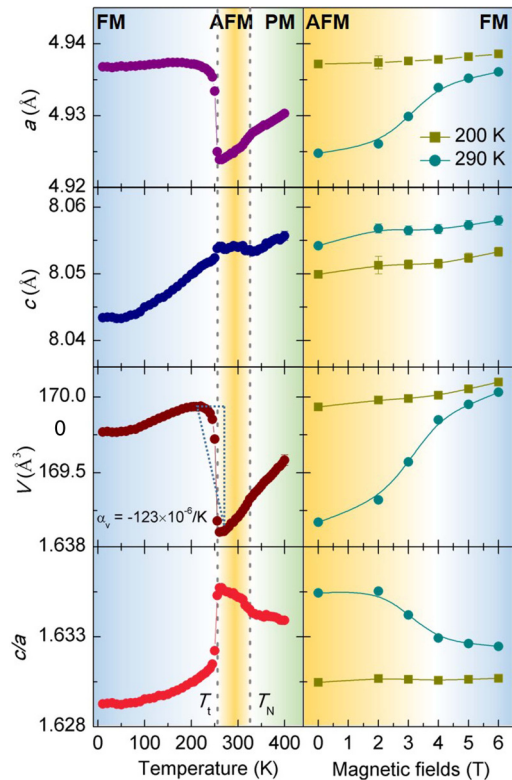


FIG. 3. The lattice constants  $a$  and  $c$ , volume  $V$ , and  $c/a$  of the unit cell as functions of temperature (left) and of magnetic fields (right). The colorful shadows schematically illustrate the individual phase zones (AFM, FM, and PM) and their crossovers (only for 290 K in the right panel). The two dotted lines label  $T_N$  of 325 K and  $T_t$  of 255 K.

lower intensity [17,18]. The magnetic representational analysis provides two collinear AFM structures in which the magnetic moments of Fe at the  $6h$  sites either align along the  $c$  direction or lie in the  $ab$  plane. However, magnetic diffraction patterns generated for these two collinear models do not agree with experiments [20]. We hence need to consider frustrated AFM structures, where magnetic moments of Fe at the  $6h$  sites form the  $120^\circ$  structure in the  $ab$  plane and interlayer coupling can be either FM or AFM. The 102 and 111 peaks can be obtained only for the interlayer AFM configuration, and thus it is the most likely model for the AFM state in our system [20]. By taking the model, we refine the diffraction data, as shown in Fig. 2(c). The determined magnetic moment is around  $0.6(1)\mu_B$ . This is much smaller than  $1.16(7)\mu_B$  of the FM state at 240 K. Such an AFM structure is actually the  $q = 0$  kagome AFM in the extended lattice, as shown in the left panel of Fig. 1(a), differing from the  $\sqrt{3} \times \sqrt{3}$  structure [33]. Moreover, the disordered moments of Fe at  $2a$  sites sandwiched by two AFM coupled  $6h$  layers might be frustrated as well. This would be the reason why the sizable moments of Fe at  $2a$  sites are not ordered.

We summarize the temperature dependencies of lattice constants  $a$  and  $c$ , the volume  $V$ , and the  $c/a$  ratio of the unit cell in the left panel of Fig. 3. When temperature goes down through  $T_N$  of 325 K, the lattice shrinks in the  $ab$  plane rather than along the  $c$  direction. The temperature dependence of  $a$

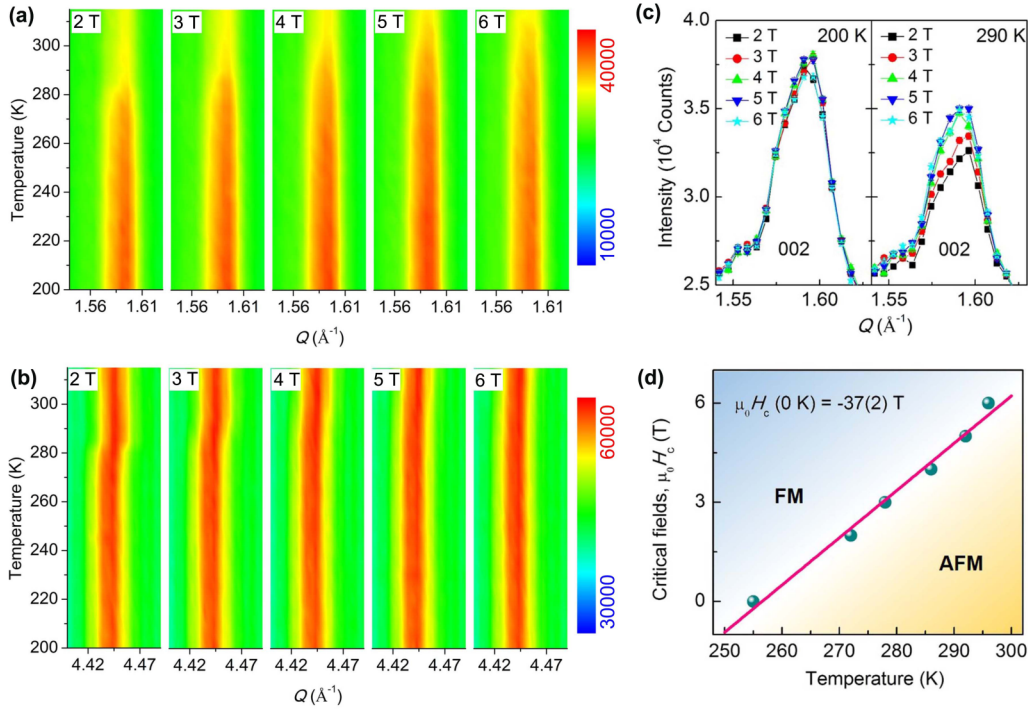


FIG. 4. (a) and (b) The contour plots of diffraction intensity of Bragg peaks 002 and 300 at different magnetic fields, respectively. (c) Bragg peak 002 at 200 K (left) and at 290 K (right). (d) The phase diagram of the first-order transition. The phase boundary is well described by a linear relation with intercept of  $-37(2)$  T.

obviously deviates from the linear relation for the PM state. This might be related to the exchange-striction effect arising from AFM ordering. At  $T_i$  of 255 K,  $a$  exhibits a large jump,  $\Delta a/a \approx 0.3\%$ , and the system transforms simultaneously to the FM state. Below  $T_i$ ,  $a$  stays nearly constant, while  $c$  gradually decreases. As shown by the slope triangle,  $V$  is increased by around 0.5% with varying temperature from 260 to 220 K, which is translated into a tremendous coefficient of volumetric thermal expansion,  $-123 \times 10^{-6}/\text{K}$ . This value is on the same order of magnitude as  $-413 \times 10^{-6}/\text{K}$  found in  $\text{Bi}_{0.95}\text{La}_{0.05}\text{NiO}_3$  in the region of 300–360 K [34]. Meanwhile,  $c/a$  changes back to the ideal value of  $\sqrt{8/3}$  geometrically defined for the hexagonal closest-packed structure after a progressive increase below  $T_N$ .

The magnetic phase competition is examined in the magnetic fields and temperature phase space by employing *in situ* neutron diffraction. The contour plots of the diffraction intensity of the 002 and 300 Bragg peaks are shown in Figs. 4(a) and 4(b), respectively. The crossover of the intensity of the 002 peak, an indication of AFM to FM transition, is prompted to higher temperatures with increasing magnetic fields. This means the AFM state is suppressed, in accordance with previous specific-heat values measured with magnetic fields [35] and our diffraction data under applied magnetic fields. At 200 K, it is FM, so that the intensity is much less susceptible to magnetic fields than at 290 K where it is AFM. The intensity at 290 K becomes almost field independent beyond 4 T, which roughly defines the critical field inducing the AFM to FM transition. In response to the applied magnetic fields, the lattice is concomitantly expanded in the  $ab$  plane, as seen in the shift of the 300 peak. The detailed field dependencies of lattice dimensions are compared with their

temperature dependencies in Fig. 3. The diffraction under *in situ* magnetic fields enables us to directly determine the magnetic phase diagram. The transition temperature is defined as one where the lattice constant  $a$  of the FM state starts to sharply drop. There is a linear relationship, depicted by the fitting shown in Fig. 4(d), similar to the other systems with AFM to FM transitions [36]. The intercept represents the extrapolated critical fields for the AFM to FM transition at 0 K.

## B. DFT calculations

The reentrant temperature dependence of  $c/a$  in the vicinity of the AFM phase reflects the magnetic phase competition and suggests the existence of an energy minimum in the energy profile with respect to the lattice dimensions, which is justified by our DFT total-energy calculation for a  $2a \times a \times c$  supercell ( $\text{Hf}_7\text{TaFe}_{16}$ ). This adopted supercell is the smallest one whose composition,  $\text{Hf}_{0.875}\text{Ta}_{0.125}\text{Fe}_2$ , can match the actual one. We consider three magnetic configurations: FM,  $120^\circ$  AFM, and PM. The FM ordering significantly lowers the total energy and expands the lattice compared with the PM state, as listed in Table I. Then, the variation of total energy in the AFM configuration is examined by the calculation varying lattice constant  $a$  when  $c$  is fixed at the FM value of 7.988 Å. It can be seen in Fig. 5(a) that the AFM arrangement prefers the in-plane contraction, as reflected by the reduced total energy when  $a$  is decreased from that of FM. However, the system is destabilized by a further compression after passing through the energy minimum. It is consequently concluded that the lattice distortion energy most likely governs the phase competition. The local energy minimum of the FM state is

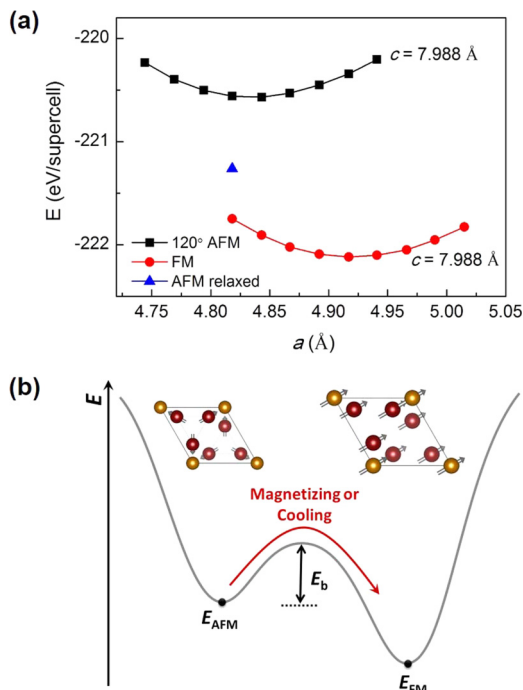


FIG. 5. (a) Total energy calculation of the frustrated AFM state and the FM state.  $c$  is fixed at 7.988 Å, which is the value for the FM state in a fully relaxed calculation. (b) Schematic diagram of the ground-state energy landscape of the first-order transition from AFM to FM states with magnetizing or cooling, whose structures are shown along the  $c$  direction.

exactly determined by the DFT calculation to be  $-222.119$  eV for the supercell. In the AFM state, symmetry breaking of the lattice is found in the fully relaxed calculation. The resulting total energy,  $-221.263$  eV [triangle in Fig. 5(a)], provides the lower bound of the total energy in the frame of DFT.

### C. Relevance to NTE

The delicate magnetic phase competition is facilitated by the magnetic frustration that manifests as the unique energy landscape schematically drawn in Fig. 5(b). Two local energy minima correspond to FM and AFM states whose structures along the  $c$  direction are shown on the top. The AFM one is less stable due to the frustration effect. They are separated by an energy barrier  $E_b$ , which is measured by magnetic Zeeman energy exerted by critical fields  $\mu_0 H_c$  (0 K). It is

estimated to be about 6 meV per chemical formula. At finite temperatures,  $E_b$  is significantly reduced by the giant magnetic fluctuation. Accordingly, this transition can be activated by a small perturbation like decreasing temperature (leading to *self-compression* due to AFM exchange-striction) or applying moderate magnetic fields. This energy profile is the origin of the colossal NTE effect.

The fluctuating nature of the AFM state is well supported by the thermodynamic measurements. On the one hand, it is evidenced by the magnetocaloric and barocaloric effects. The entropy change at the magnetic-field-induced AFM to FM transition is negative [37], while it is positive at the pressure-induced FM to AFM transition inferred by the volumetric Clausius-Clapeyron relation with  $dT_t/dP = -130$  K/GPa [38,39]. The Debye temperature is almost composition independent when  $x$  is changed from 0 to 0.5 in  $\text{Hf}_{1-x}\text{Ta}_x\text{Fe}_2$ , which correspond to FM and AFM ground states, respectively, so that the observed entropy changes originate mostly from the magnetic subsystem [40]. They are clearly indicative of stronger disorder in the AFM state. On the other hand, the electronic specific-heat coefficient  $\gamma$  of the AFM state in  $\text{Hf}_{1-x}\text{Ta}_x\text{Fe}_2$  also suggests the giant spin fluctuation. It is determined to be  $40$  mJ/K<sup>2</sup>, nearly two times larger than that of the FM state (about  $20$  mJ/K<sup>2</sup>) as well as that of the crystallographically isostructural but magnetically nonfrustrated AFM  $\text{TiFe}_2$  ( $22$  mJ/K<sup>2</sup>) [41,42]. This discrepancy might be attributed to the magnetic frustration. In highly frustrated (Y, Sc)Mn<sub>2</sub>, similarly, an enormously large  $\gamma$ ,  $150$  mJ/K<sup>2</sup>, is observed [12].

## IV. SUMMARY

To summarize, the complete crystal and magnetic structures of  $\text{Hf}_{0.86}\text{Ta}_{0.14}\text{Fe}_2$  are determined by using neutron powder diffraction. The magnetic phase competition, enabled by the magnetic frustration, is well demonstrated in  $\mu_0 H$ - $T$  phase space. The lattice distortion is revealed to dominate the magnetic phase competition, as seen in the reentrant behavior of  $c/a$ , supported by DFT calculations. The interplay of the FM and AFM interactions with the lattice distortion leads to the colossal volumetric variations of the unit cell in response to the changes in temperature and magnetic field. This suggests that tailoring competing magnetic phases on frustrated lattices is an effective route to NTE, and it is worthwhile to extend such a scenario to other related compounds.

TABLE I. Comparison of lattice dimensions from experiments and the DFT calculations for three magnetic states. The first row is for calculated values, while the second one is for experimental values at selected temperatures. The calculations are based on the  $2a \times a \times c$  supercell.

States	$E$ (eV)	$a$ (Å)	$c$ (Å)	$V$ (Å <sup>3</sup> )	$c/a$	$M_{2a}$ ( $\mu_B$ )	$M_{6h}$ ( $\mu_B$ )
PM	$-220.491$	4.812	7.980	320.02	1.658	0	0
	(400 K)	4.9303(4)	8.0557(7)	169.583(35)	1.6339	0	0
FM	$-222.119$	4.917	7.988	335.51	1.625	1.75	1.76
	(10 K)	4.9368(4)	8.0434(5)	169.770(9)	1.6293	1.42(7)	1.42(7)
AFM	$-220.57$	4.843	7.988	324.51	1.649	0.2	1.19
	(260 K)	4.9239(4)	8.0541(4)	169.108(8)	1.6357	0	0.6(1)

## ACKNOWLEDGMENTS

The authors acknowledge the merit award of instrument time at the OPAL reactor of ANSTO. X.H.L., W.J.R., and Z.D.Z. were supported by the National Natural Science Foun-

datation of China (Grants No. 51331006 and No. 51531008). Work at UCI was supported by DOE-BES (Grant No. DE-FG02-05ER46237). Computer simulations were performed at the U.S. Department of Energy Supercomputer Facility (NERSC).

- 
- [1] M. Imada, A. Fujimori, and Y. Tokura, *Rev. Mod. Phys.* **70**, 1039 (1998).
- [2] E. Dagotto, *Science* **309**, 257 (2005).
- [3] K. A. Gschneidner, Jr., V. K. Pecharsky, and A. O. Tsokol, *Rep. Prog. Phys.* **68**, 1479 (2005).
- [4] S. B. Roy, *J. Phys. Condens. Matter* **25**, 183201 (2013).
- [5] L. Balents, *Nature (London)* **464**, 199 (2010).
- [6] C. Lacroix, P. Mendels, and F. Mila, *Introduction to Frustrated Magnetism: Materials, Experiments, Theory* (Springer, New York, 2011).
- [7] J. S. Gardner, M. J. P. Gingras, and J. E. Greedan, *Rev. Mod. Phys.* **82**, 53 (2010).
- [8] Y. Motome and N. Furukawa, *Phys. Rev. Lett.* **104**, 106407 (2010).
- [9] S.-H. Lee, H. Takagi, D. Louca, M. Matsuda, S. Ji, H. Ueda, Y. Ueda, T. Katsufuji, J.-H. Chung, S. Park, S.-W. Cheong, and C. Broholm, *J. Phys. Soc. Jpn.* **79**, 011004 (2010).
- [10] A. P. Ramirez, C. L. Broholm, R. J. Cava, and G. R. Kowach, *Phys. B (Amsterdam, Neth.)* **280**, 290 (2000).
- [11] Y. Nakamura, *J. Magn. Magn. Mater.* **31-34**, 829 (1983).
- [12] M. Shiga, K. Fujisawa, and H. Wada, *J. Phys. Soc. Jpn.* **62**, 1329 (1993).
- [13] K. Takenaka and H. Takagi, *Appl. Phys. Lett.* **87**, 261902 (2005).
- [14] J. Hemberger, H.-A. Krug von Nidda, V. Tsurkan, and A. Loidl, *Phys. Rev. Lett.* **98**, 147203 (2007).
- [15] Y. Nishihara and Y. Yamaguchi, *J. Phys. Soc. Jpn.* **52**, 3630 (1983).
- [16] H. R. Rechenberg, L. Morellon, P. A. Algarabel, and M. R. Ibarra, *Phys. Rev. B* **71**, 104412 (2005).
- [17] H. G. M. Duijn *et al.*, *J. Appl. Phys.* **81**, 4218 (1997).
- [18] L. V. Diop, O. Isnard, E. Suard, and D. Benea, *Solid State Commun.* **229**, 16 (2016).
- [19] J. Chen, L. Hu, J.-X. Deng, and X.-R. Xing, *Chem. Soc. Rev.* **44**, 3522 (2015).
- [20] See Supplemental Material at <http://link.aps.org/supplemental/10.1103/PhysRevB.93.224405> for x-ray diffraction patterns and simulated magnetic diffraction patterns with different FM and AFM models.
- [21] A. J. Studer, M. E. Hagen, and T. J. Noakes, *Phys. B (Amsterdam, Neth.)* **385-386**, 1013 (2006).
- [22] K.-D. Liss, B. Hunter, M. Hagen, T. Noakes, and S. Kennedy, *Phys. B (Amsterdam, Neth.)* **385-386**, 1010 (2006).
- [23] J. Rodriguez-Carvajal, *Phys. B (Amsterdam, Neth.)* **192**, 55 (1993).
- [24] A. S. Wills, *Phys. B (Amsterdam, Neth.)* **276-278**, 680 (2000).
- [25] G. Kresse and J. Furthmuller, *Phys. Rev. B* **54**, 11169 (1996).
- [26] G. Kresse and J. Hafner, *Phys. Rev. B* **49**, 14251 (1994).
- [27] G. Kresse and J. Hafner, *Phys. Rev. B* **47**, 558 (1993).
- [28] G. Kresse and J. Furthmuller, *Comput. Mater. Sci.* **6**, 15 (1996).
- [29] J. P. Perdew, K. Burke, and M. Ernzerhof, *Phys. Rev. Lett.* **77**, 3865 (1996).
- [30] G. Kresse and D. Joubert, *Phys. Rev. B* **59**, 1758 (1999).
- [31] P. E. Blöchl, *Phys. Rev. B* **50**, 17953 (1994).
- [32] P.-W. Ma and S. L. Dudarev, *Phys. Rev. B* **91**, 054420 (2015).
- [33] A. Chubukov, *Phys. Rev. Lett.* **69**, 832 (1992).
- [34] M. Azuma *et al.*, *Nat. Commun.* **2**, 347 (2011).
- [35] P. Bag, R. Rawat, P. Chaddah, P. D. Babu, and V. Siruguri, *Phys. Rev. B* **93**, 014416 (2016).
- [36] B. Li *et al.*, *Appl. Phys. Lett.* **100**, 242408 (2012).
- [37] Z. Han *et al.*, *J. Alloys Compd.* **377**, 75 (2004).
- [38] L. Morellon, P. A. Algarabel, M. R. Ibarra, Z. Arnold, and J. Kamard, *J. Appl. Phys.* **80**, 6911 (1996).
- [39] D. Matsunami, A. Fujita, K. Takenaka, and M. Kano, *Nat. Mater.* **14**, 73 (2015).
- [40] H. Wada, N. Shimamura, and M. Shiga, *Phys. Rev. B* **48**, 10221 (1993).
- [41] P. J. Brown, J. Deportes, and B. Ouladdiaf, *J. Phys. Condens. Matter* **4**, 10015 (1992).
- [42] H. Wada, M. Hada, M. Shiga, and Y. Nakamura, *J. Phys. Soc. Jpn.* **59**, 701 (1990).